Chapter 4

Phonon Modes and Elastic Properties of Zr-Based Bulk Metallic Glasses: A Pseudopotential Approach

Punitkumar Harshadbhai Suthar

Additional information is available at the end of the chapter

http://dx.doi.org/10.5772/intechopen.79568

Abstract

The collective dynamics for longitudinal and transverse phonon modes and elastic properties are studied for bulk metallic glasses (BMGs) using Hubbard-Beeby approach along with our well establishes model potential. The important ingredients in the present study are the pair-potential and local field correlation function. The local field correlation functions due to Hartree (H), Taylor (T), Ichimaru and Utsumi (IU), Farid et al. (F), Sarkar et al. (S) and Hubbard and Sham (HS) are employed to investigate the influence of the screening effects on the vibrational dynamics of Zr-Ti-Cu-Ni-Be, Zr-Cu-Ni-Al-Ta, Zr-Ti-Cu-Ni-Al and Zr-Al-Ni-Cu. The result for the elastic constants like bulk modulus B_T, rigidity modulus G, Poisson's ratio ξ, Young's modulus Y, Debye temperature Θ_D, the propagation velocity of elastic waves and dispersion curves are found to be in good agreement with experimental and other available data. The present results are consistent and confirm the applicability of model potential and self-consistent phonon theory for such studies.

Keywords: bulk metallic glass, pseudopotential, local field correction function, phonon modes, elastic properties

1. Introduction

Bulk metallic glass-forming liquids are alloys with typically three to five metallic components that have large atomic size mismatch and a composition close to a deep eutectic [1]. Metallic glasses have regained considerable interest due to the fact that new glass forming composition have been found that have a critical cooling rate of less than 100 K s^{-1} and can be made glassy with dimensions of 1 cm or more. The development of such alloys with a very high resistance to crystallization of the under cooled melt has opened new opportunities for the primary study

of both the liquid state and the glass transition. The ability of bulk specimens has enabled measurements of various physical, particularly mechanical, properties that were previously impossible. Furthermore, these alloys are progressively being used for engineering applications. This new class of material is normally referred to as "bulk metallic glasses." [1–10]

Bulk metallic glass an excellent glass forming ability and high thermal stability have attracted much attention in the recent years. It has also occupied an important position due to their unique physical properties and technological importance. Zr-based BMGs are the coming up candidates to replace the usual materials used in the industry as a result of their superior mechanical properties, for example strength, hardness, toughness and elasticity [2–10]. Recently formation of Zr-Ti-Cu-Ni-Be, Zr-Ti-Cu-Ni-Be, Zr-Cu-Ni-Al-Ta, Zr-Ti-Cu-Ni-Al and Zr-Al-Ni-Cu bulk metallic glass (BMGs) alloys distinguished itself from other metallic alloys by extraordinary glass forming ability (GFA) [4–9]. These alloys have opened the possibility to study the nature of glass transition in BMGs, offered the potential of BMGs as new generation engineering materials and controllable properties is one of the central issues in the condensed matter physics and material sciences [2–10]. Metallic glass alloys are normally regarded as elastically isotopic, and they behave as an elastic continuum at low temperatures, with well-defined dispersion relation so that ultrasonic waves propagated through it. Perker and Johnson [9] are made an important process of the design of the Zr–Ti–Cu–Ni–Be ($Zr_{41}Ti_{14}Cu_{12.5}Ni_{10}Be_{22.5,}$ $Zr_{45.4}Ti_{9.6}Cu_{10.15}Ni_{8.6}Be_{26.25,}$ and $Zr_{46.75}Ti_{8.25}Cu_{7.5}Ni_{10}Be_{27.5}$) five different concentration, Zr-Cu-Ni-Al glass-forming alloy family. This family has distinct glass transition, very high stability of supercooled liquid state and exhibits high thermal stability against crystallization. Dissolution of minute amount of metalloid elements into the Zr-base system can enlarge the thermal stability and hardness of the BMG. Zr-based BMGs are used in manufacturing of industrial production [4–9]. Recently, Agarwal has reported the phonon dispersion curves of Zr-Ti-Cu-Ni-Be BMGs using Bhatia and Singh (BS) approach [11]. Wang et al. [4–6] have represented elastic properties using ultrasonic method. In the present study, we have investigated theoretically, phonon dispersion curve and elastic properties of Zr-based [4–10] bulk metallic glasses with the help of pseudopotential formalism and along with Hubbard and Beeby [12] approach and employing pseudopotential formalism along with the five different local field correction functions due to Hartree [13], Taylor [14], Ichimaru and Utsumi [15], Farid et al. [16], Sarkar et al. [17].

2. Theory

There are three main theoretical approaches used to compute the phonon frequency of binary alloys: one is Hubbard and Beeby (HB) [12], second is Takeno and Goda (TG) [18], and last is Bhatia and Singh (BS) [11]. The HB approach is the random phase approximation according to this theory, a liquid random from a crystalline solid in two principal ways. Initially, the atoms in the metallic glasses do not form a regular array, i.e. they disordered. So the HB theoretical models have been employed to generate the phonon dispersion curve and their related properties of bulk metallic glass alloys in the present computation.

http://dx.doi.org/10.5772/intechopen.79568

The effective ion-ion interaction is given as

$$V(r) = \frac{Z^2 e^2}{r} + \frac{2}{\pi}\int dqF(q)\exp\left(-iq\cdot r\right) \tag{1}$$

where $F(q)$ is the characteristic energy wave number. The first and second terms in the above expression are due to the coulomb interaction between ion and indirect interaction through the conduction electrons, respectively; q is the q-space wave vector, e is the charge of an electron. In the present study, we have considered the effective atom approach to compute the phonon dispersion curve (PDC). For the present study, we have used the Jani et al. [19–21] model potential in q-space is given as,

$$W_B^{eff}(q) = -\frac{4\pi^2 e^2}{\Omega_0 q^2}\left(\cos\left(qr_c^{eff}\right) - \frac{\exp\left(-1\right)\ qr_c^{eff}}{1+\left(qr_c^{eff}\right)^2}\left(\sin\left(qr_c^{eff}\right) + qr_c^{eff}\cos\left(qr_c^{eff}\right)\right)\right) \tag{2}$$

The characteristic feature of this model potential is the single parametric nature. r_c^{eff} is the potential parameter. This determination of parameter is independent of any fitting procedure with the observed quantities. The energy wave number characteristics in expression (1) are given by [21–25]

$$F(q) = -\frac{\Omega_{0eff} q^2}{16\pi}\left|W_B^{eff}(q)\right|^2 \times \frac{\left[\varepsilon_H^{eff}(q)-1\right]}{\left[1+\left(\varepsilon_H^{eff}(q)-1\right)\left(1-f_{eff}(q)\right)\right]} \tag{3}$$

Here $W_B^{eff}(q)$ is the effective bare ion potential, $\varepsilon_{\mathrm{H}}^{\mathrm{eff}}(q)$is the Hartree dielectric response function and $f_{eff}(q)$ is the local field correction function (LFCF) due to the Hartree (H) [13], Taylor (T) [14], Ichimaru-Utsumi (IU) [15], Farid et al. (F) [16] and Sarkar et al. (S) [17] are used here to include the effect of screening on the collective modes of bulk metallic glasses Zr-Ti-Cu-Ni-Be BMG for five different concentration, Zr-Cu-Ni-Al-Ta BMG, Zr-Ti-Cu-Ni-Al BMG and Zr-Al--Ni-Cu BMG for three different concentration. Long-wavelength limits of the phonon modes are then used to investigate the elastic properties, viz. longitudinal sound velocity, transverse sound velocity, Debye temperature, isothermal bulk modulus, modulus of rigidity, Poisson's ratio and Young's modulus. Five different types of LFCF are employed here for the study of the effect of exchange and correlation on the aforesaid properties. Pair potential or effective interaction is realized through interatomic potential, ion-ion potential and electron-electron potential developed between two similar particles like atoms, ion and electrons. The pair-correlation function g(r) is equally important as the pair potential. It contains useful information about the inter particle radial correlation and structure which in turn decides the electrical thermodynamically and amorphous materials.

The effective potential and pair correlation function $g(r)$ are the used to calculate the longitudinal and transverse phonon frequencies. The product of the static pair-correlation function $g(r)$ and the second derivative of the interatomic potential $V_{eff}^{''}(r)$ are peaked at σ, which is the

hard sphere diameter. The longitudinal phonon frequency ω_l (q) and transverse phonon frequency ω_t(q) are given by the expression due to Hubbard and Beeby (HB).

$$\omega_l^2(q) = \omega_E^2\left[1 - \frac{3\sin(q\sigma)}{q\sigma} - \frac{6\cos(q\sigma)}{(q\sigma)^2} + \frac{6\sin(q\sigma)}{(q\sigma)^3}\right] \tag{4}$$

and

$$\omega_t^2(q) = \omega_E^2\left[1 + \frac{3\cos(q\sigma)}{(q\sigma)^2} - \frac{6\sin(q\sigma)}{(q\sigma)^3}\right] \tag{5}$$

where

$$\omega_E = \frac{4\pi n_{eff}}{3M_{eff}}\int_0^\infty g(r)r^2V_{eff}^{''}(r)dr \tag{6}$$

$$V_{eff}''(r) = \frac{4Z^2}{r^3} + \frac{\Omega_0}{\pi^2}\int_0^\infty F(q)q^2\left[\frac{2\sin(qr)}{qr^3} - \frac{2\cos(qr)}{r^2} - \frac{q\sin(qr)}{r}\right]dq, \tag{7}$$

and

$$g(r) = \exp\left[\left(\frac{-V_{eff}''(r)}{k_BT}\right) - 1\right] \tag{8}$$

Here, ρ is the number density, M is the atomic mass, g(r) is the pair correlation function, Ω_0 is the atomic volume, F(q) and S(q) be the energy wave number characteristic and the structure factor of the element, respectively.

In the long-wavelength limit, the phonon dispersion curve shows an elastic behavior. Hence, the longitudinal ν_l and transverse ν_t sound velocities are also calculated by [22–25]

$$\omega_L\ \alpha\ q \text{ and } \omega_T\ \alpha\ q, \therefore \omega_L = v_l q \text{ and } \omega_T = v_l q \tag{9}$$

Various elastic properties are determined by the longitudinal and transverse phonon frequencies.

The bulk modulus B, Poisson's ratio 'ξ', modulus of rigidity G, Young's modulus Y and the Debye temperature θ_D are calculated using the expression below [22–25]

$$B = \rho\left(v_l^2 - \frac{4}{3}v_t^2\right) \tag{10}$$

ρ is the isotropic density of the solid,

$$\xi = \frac{1 - 2\left(v_t^2/v_l^2\right)}{2 - 2\left(v_t^2/v_l^2\right)} \tag{11}$$

$$G = \rho\, v_t^2 \tag{12}$$

$$Y = 2G(\xi + 1) \tag{13}$$

and

$$\theta_D = \frac{h}{k_B}\left[\left(\frac{9\rho}{4\pi}\right)^{1/3}\left(\frac{1}{v_l^3}+\frac{2}{v_t^3}\right)^{-1/3}\right] \tag{14}$$

where 'h' is Plank constant and k_B is the Boltzmann constant.

3. Results and discussion

The input parameters and constants used in the present computation are shown in **Table 1**. Pair potential (**Figures 1(a)–10(a)**) and the phonon frequencies of longitudinal and transverse branch (**Figures 1(b)–10(b)**) of various bulk metallic glasses are shown in **Figures 1–10**. Our well-established model potential is used along with five different local field correction functions to computed form factors and thereby effective pair potentials. The phenomenological approach of Hubbard and Beeby [8, 12, 21–25] is used further to compute phonon frequencies. The longitudinal and transverse phonon frequencies show all broad features of collective excitations of all BMGs. It is seen from the results of phonon frequencies that the nature of peak positions are not much affected by different screening functions, but both the longitudinal and transverse frequencies show deviation for H, T and S functions with respect to IU and F screening function for present model potential. At large momentum, phonons from longitudinal branch are found responsible for momentum transfer. Phonons of transverse branch undergo large thermal modulation due to the anharmonicity of lattice vibrations in this branch. The first minimum in the longitudinal branch corresponds to umklapped scattering process. No experimental data of structure factor for these BMGs are available. In the long wavelength limit, the frequencies are elastic and allow us to computed elastic constants.

BMGs	Z_{eff}	Ω_{eff} (au)^3	r_c^{eff} (au)	M_{eff} (amu)	r_{seff} (au)
$Zr_{38.5}Ti_{16.5}Cu_{15.25}Ni_{9.75}Be_{20}$	3.100	115.447	1.0565	60.237	2.0716
$Zr_{41}Ti_{14}Cu_{12.5}Ni_{10}Be_{22.5}$	3.100	119.893	1.0699	59.945	2.0978
$Zr_{44}Ti_{11}Cu_{10}Ni_{10}Be_{25}$	3.100	119.809	1.0696	59.882	2.0974
$Zr_{45.4}Ti_{9.6}Cu_{10.15}Ni_{8.6}Be_{26.25}$	3.100	123.501	1.0805	59.875	2.1187
$Zr_{46.75}Ti_{8.25}Cu_{7.5}Ni_{10}Be_{27.5}$	3.100	124.510	1.0834	59.710	2.1245
$Zr_{52.25}Cu_{28.5}Ni_{4.75}Al_{9.5}Ta_5$	2.957	128.860	1.1133	80.173	2.1830
$Zr_{57}Ti_5Cu_{20}Ni_8Al_{10}$	3.040	127.676	1.0385	74.493	2.1560
$Zr_{61.88}Al_{10}Ni_{10.12}Cu_{18}$	3.056	127.039	1.0960	76.143	2.1459
$Zr_{64.13}Al_{10}Ni_{10.12}Cu_{15.75}$	3.124	130.140	1.0968	76.874	2.1505
$Zr_{65}Al_{10}Ni_{10}Cu_{15}$	3.150	135.985	1.1099	77.395	2.1762

Table 1. Input parameters and constants.

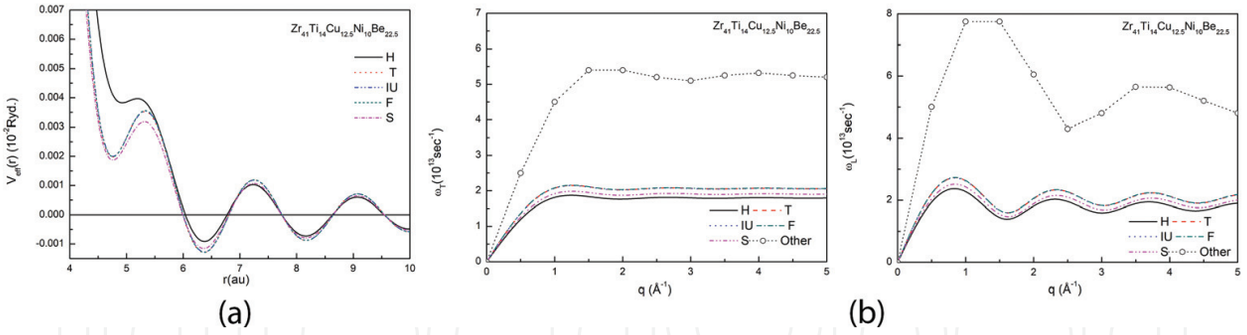

Figure 1. (a) Pair potential for $Zr_{41}Ti_{14}Cu_{12.5}Ni_{10}Be_{22.5}$ BMG. (b) Phonon dispersion curve (ω_L & ω_T) for $Zr_{41}Ti_{14}Cu_{12.5}Ni_{10}Be_{22.5}$ BMG along with other available data [8].

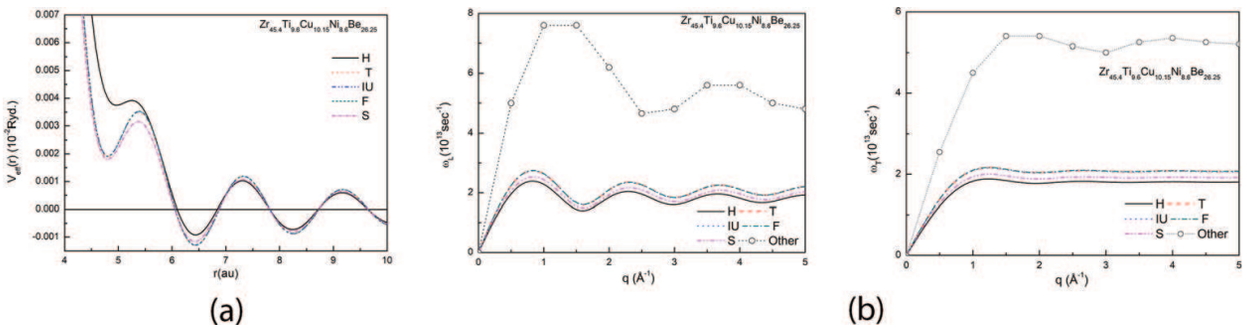

Figure 2. (a) Pair potential for $Zr_{45.4}Ti_{9.6}Cu_{10.15}Ni_{8.6}Be_{26.25}$ BMG. (b) Phonon dispersion curve (ω_L & ω_T) of $Zr_{45.4}Ti_{9.6}Cu_{10.15}Ni_{8.6}Be_{26.25}$ BMG along with other available data [8].

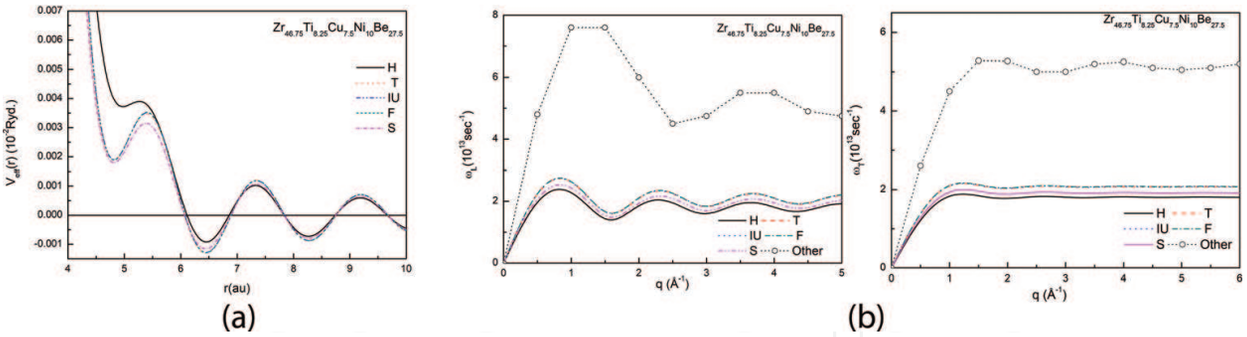

Figure 3. (a) Pair potential for $Zr_{46.75}Ti_{14}Cu_{12.5}Ni_{10}Be_{22.5}$ BMG. (b) Phonon dispersion curve (ω_L & ω_T) of $Zr_{46.75}Ti_{14}Cu_{12.5}Ni_{10}Be_{22.5}$ BMG, along with other available data [8].

3.1. Zr-Ti-Cu-Ni-Be BMG ($Zr_{41}Ti_{14}Cu_{12.5}Ni_{10}Be_{22.5}$, $Zr_{45.4}Ti_{9.6}Cu_{10.15}Ni_{8.6}Be_{26.25}$, $Zr_{46.75}Ti_{8.25}Cu_{7.5}Ni_{10}Be_{27.5}$, $Zr_{44}Ti_{11}Cu_{10}Ni_{10}Be_{25}$, $Zr_{38.5}Ti_{16.5}Ni_{9.75}Cu_{15.25}Be_{20}$)

Equation to compute phonon frequency and longitudinal and transverse sound velocity are taken from Thakore et al. [21, 23]. Pair potential and the phonon modes computed for $Zr_{41}Ti_{14}Cu_{12.5}Ni_{10}Be_{22.5}$ BMG, $Zr_{45.4}Ti_{9.6}Cu_{10.15}Ni_{8.6}Be_{26.25}$ BMG, $Zr_{46.75}Ti_{8.25}Cu_{7.5}Ni_{10}Be_{27.5}$

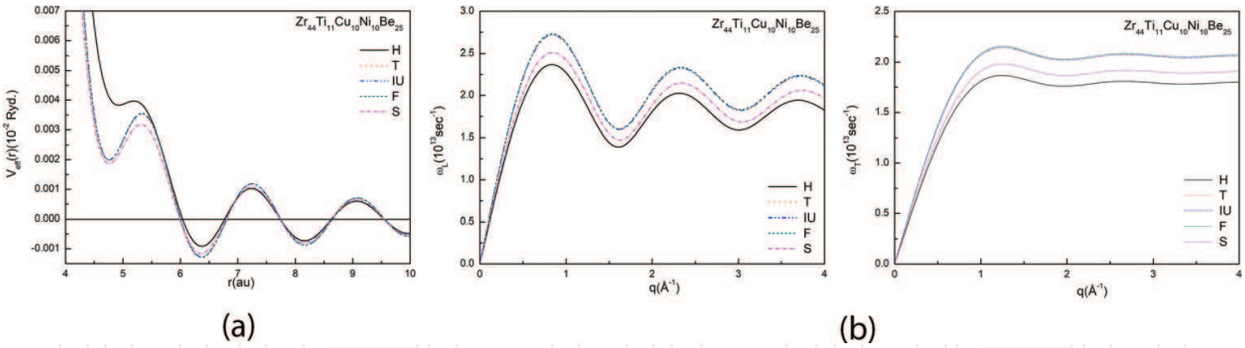

Figure 4. (a) Pair potential for $Zr_{44}Ti_{11}Cu_{10}Ni_{10}Be_{25}$ BMG. (b) Phonon dispersion curve (ω_L & ω_T) for $Zr_{44}Ti_{11}Cu_{10}Ni_{10}Be_{25}$ BMG.

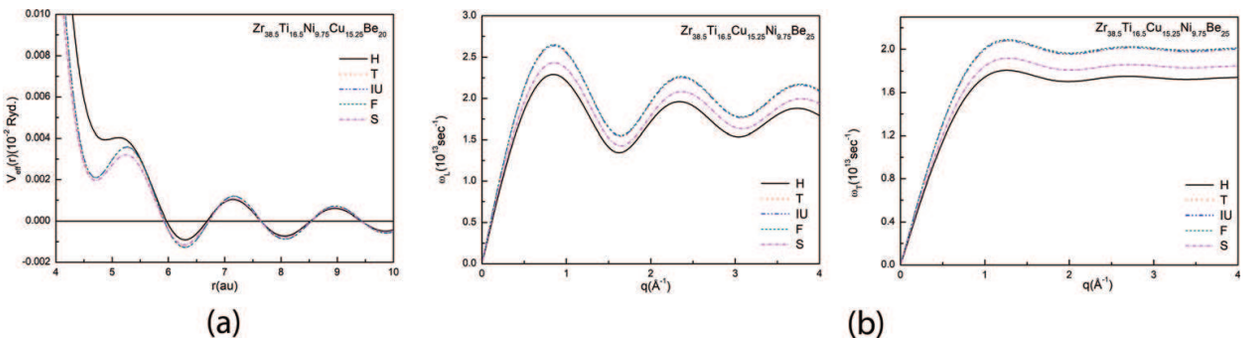

Figure 5. (a) Pair potential for $Zr_{38.5}Ti_{16.5}Cu_{15.25}Ni_{9.75}Be_{25}$ BMG. (b) Phonon dispersion curve (ω_L & ω_T) for $Zr_{38.5}Ti_{16.5}Cu_{15.25}Ni_{9.75}Be_{25}$ BMG.

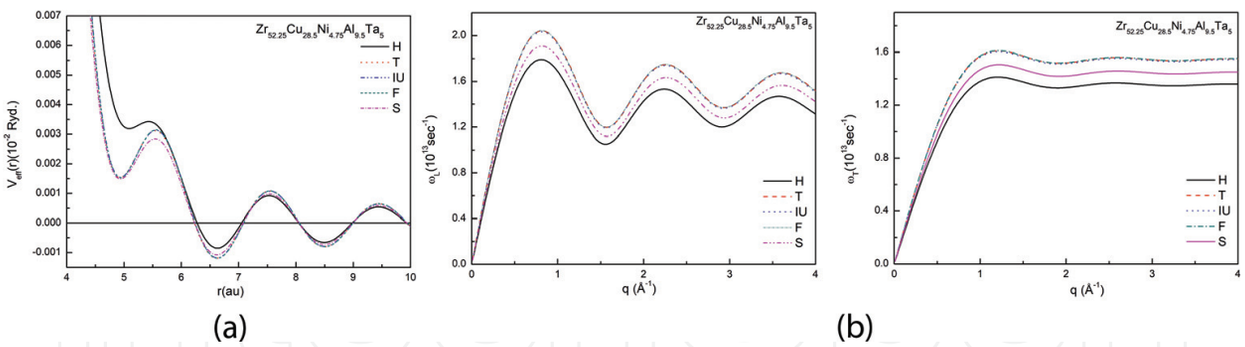

Figure 6. (a) Pair potential for $Zr_{52.25}Cu_{28.5}Ni_{4.75}Al_{9.5}Ta_5$ BMG. (b) Phonon dispersion curve (ω_L & ω_T) for $Zr_{52.25}Cu_{28.5}Ni_{4.75}Al_{9.5}Ta_5$ BMG.

BMG, $Zr_{44}Ti_{11}Cu_{10}Ni_{10}Be_{25}$ BMG, $Zr_{38.5}Ti_{16.5}Ni_{9.75}Cu_{15.25}Be_{20}$ BMG are shown in **Figures 1–5** respectively. It is observed that the study reveals the general trends of the pair potential for BMGs considered here, suggesting that the position of the first minima is affected by the type of screening functions. The maximum depth in the pair potential in the present study is obtained due to S screening function for $Zr_{41}Ti_{14}Cu_{12}Ni_{10}Be_{22.5}$, $Zr_{45.4}Ti_{9.6}Cu_{10.15}Ni_{8.6}Be_{26.25}$ and $Zr_{46.75}Ti_{8.25}Cu_{7.5}Ni_{10}Be_{27.5}$ BMGs. From **Figures 2–4** it is seen from the results of phonon frequencies that the general nature and peak positions are not affected very much by different

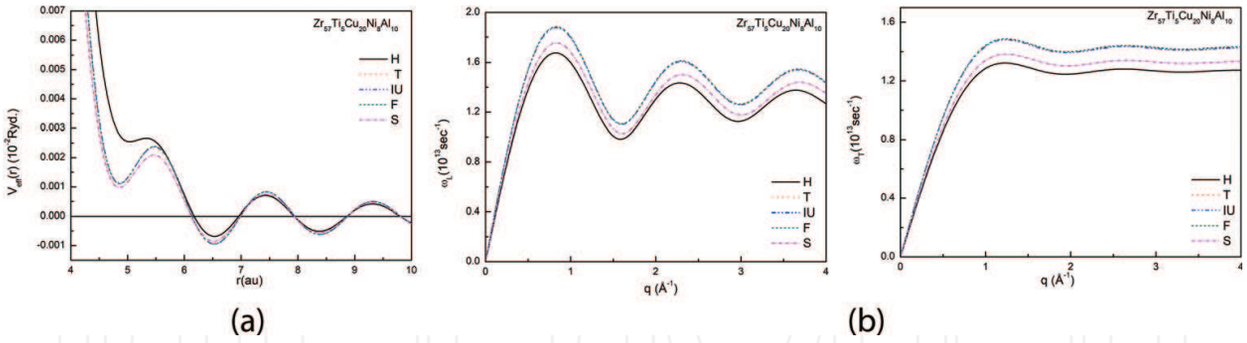

Figure 7. (a) Pair potential for $Zr_{57}Ti_5Cu_{20}Ni_8Al_{10}$ BMG. (b) Phonon dispersion curve (ω_L & ω_T)) for $Zr_{57}Ti_5Cu_{20}Ni_8Al_{10}$ BMG.

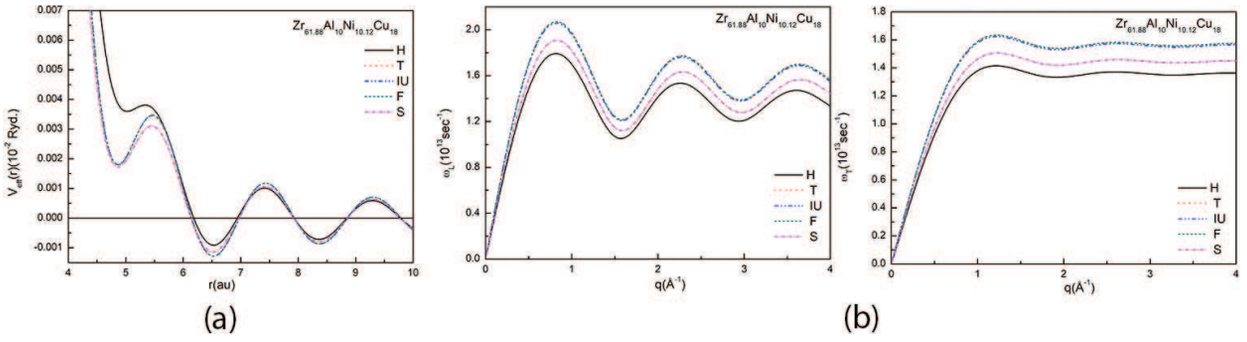

Figure 8. (a) Pair potential for $Zr_{61.88}Al_{10}Ni_{10.12}Cu_{18}$ BMG. (b) Phonon dispersion curve (ω_L & ω_T) for $Zr_{61.88}Al_{10}Ni_{10.12}Cu_{18}$ BMG.

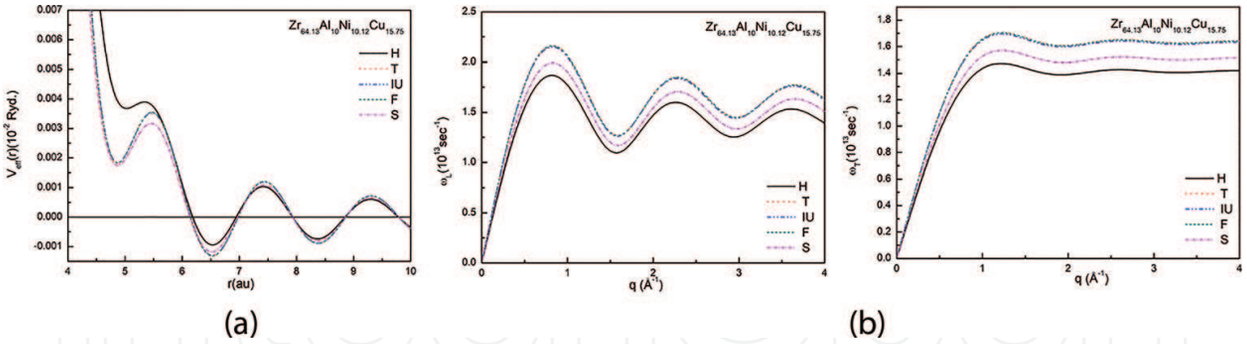

Figure 9. (a) Pair potential for $Zr_{64.13}Al_{10}Ni_{10.12}Cu_{15.75}$ BMG. (b) Phonon dispersion curve (ω_L & ω_T) for $Zr_{64.13}Al_{10}Ni_{10.12}Cu_{15.75}$ BMG.

screening functions, but magnitude of both the longitudinal and transverse frequencies show deviation with respect to screening function. From the **Figures 2–6** that the oscillations are prominent in the longitudinal mode as compared to transverse mode, which indicates that the collective excitations at larger wave vector transfer due to the dispersion of longitudinal excitation. The maximum and minimum percentile deviation for the elastic properties of bulk modulus, modulus of rigidity, Young modulus and Debye temperature with respect to the experimental data from **Tables 2–4**. For bulk modulus, the computed percentile maximum

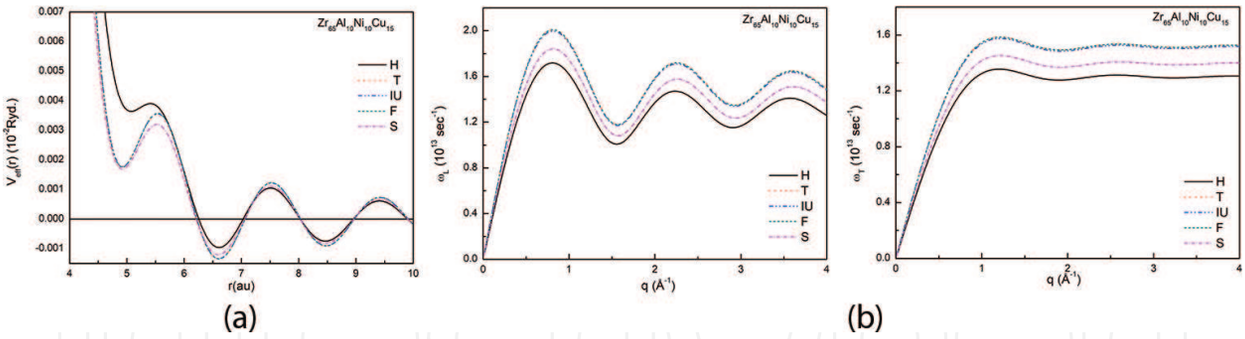

Figure 10. (a) Pair potential for $Zr_{65}Al_{10}Ni_{10}Cu_{15}$ BMG. (b) Phonon dispersion curve (ω_L & ω_T) for $Zr_{65}Al_{10}Ni_{10}Cu_{15}$ BMG.

Properties	H [13]	T [14]	IU [15]	F [16]	S [17]	Exp. [4–6]	Other [4–6]
$\upsilon_L \times 10^5$ (cm s^{-2})	4.553	5.177	5.176	5.203	4.776	—	5.174
$\upsilon_T \times 10^5$ (cm s^{-2})	2.629	2.989	2.988	3.004	2.757	—	2.472
$B_T \times 10^{12}$ (dyne/cm^2)	0.645	0.834	0.834	0.842	0.701	1.148 1.141	1.150
$G \times 10^{12}$ (dyne/cm^2)	0.387	0.501	0.500	0.505	0.426	0.374	0.471
ξ	0.25	0.25	0.25	0.25	0.25	0.35	0.352
$Y \times 10^{12}$ (dyne/cm^2)	0.966	1.251	1.251	1.263	1.065	1.013 1.012	1.055
θ_D (K)	333.0	378.7	378.7	380.6	349.4	—	327

Table 2. Elastic properties of $Zr_{41}Ti_{14}Cu_{12.5}Ni_{10}Be_{22.5}$ BMG.

Properties	H [13]	T [14]	IU [15]	F [16]	S [17]	Exp.	Other [4–6]
$\upsilon_L \times 10^5$ (cm s^{-2})	4.621	5.253	5.249	5.277	4.850	—	5.171
$\upsilon_T \times 10^5$ (cm s^{-2})	2.668	3.033	3.031	3.047	2.800	—	2.485
$B_T \times 10^{12}$ (dyne/cm^2)	0.644	0.833	0.832	0.840	0.709	—	1.119
$G \times 10^{12}$ (dyne/cm^2)	0.386	0.499	0.499	0.504	0.426	—	0.373
ξ	0.25	0.25	0.25	0.25	0.25	—	0.35
$Y \times 10^{12}$ (dyne/cm^2)	0.966	1.249	1.247	1.260	1.065	—	1.009
θ_D (K)	334.7	380.5	380.2	382.2	351.3	—	327

Table 3. Elastic properties for $Zr_{45.4}Ti_{9.6}Cu_{10.15}Ni_{8.6}Be_{26.25}$ BMG.

deviation with respect to experimental data is found in H functions, the values are 43.82, 42.42 and 43.48% and minimum deviation is found in F functions, the values are 26.69, 24.92 and 26.25% for $Zr_{41}Ti_{14}Cu_{12}Ni_{10}Be_{22.5}$, $Zr_{45.4}Ti_{9.6}Cu_{10.15}Ni_{8.6}Be_{26.25}$ and $Zr_{46.75}Ti_{8.25}Cu_{7.5}Ni_{10}Be_{27.5}$ BMGs respectively. The computed percentile deviation for modulus of rigidity with respect to experimental data, the maximum deviation is found to be 35.54, 35.12 and 42.55% of F

functions and minimum deviation is found in H function, the values are 3.47, 3.47 and 9.26% for $Zr_{41}Ti_{14}Cu_{12}Ni_{10}Be_{22.5}$, $Zr_{45.4}Ti_{9.6}Cu_{10.15}Ni_{8.6}Be_{26.25}$ and $Zr_{46.75}Ti_{8.25}Cu_{7.5}Ni_{10}Be_{27.5}$ BMGs respectively. For Young modulus, the computed percentile maximum deviation with respect to experimental data is found in F functions, the values are 24.72, 24.90 and 24.74% and minimum deviation is found in H functions, the values are 4.49, 4.22 and 7.47%, for $Zr_{41}Ti_{14}Cu_{12}Ni_{10}Be_{22.5}$, $Zr_{45.4}Ti_{9.6}Cu_{10.15}Ni_{8.6}Be_{26.25}$ and $Zr_{46.75}Ti_{8.25}Cu_{7.5}Ni_{10}Be_{27.5}$ BMGs respectively. Similarly for Debye temperature, the computed percentile maximum deviation with respect to experimental data is found in F function, the values are 16.39, 16.90 and 16.33% and minimum deviation is found in H function, the values are 1.86, 2.36 and 2.37%, for $Zr_{41}Ti_{14}Cu_{12}Ni_{10}Be_{22.5}$, $Zr_{45.4}Ti_{9.6}Cu_{10.15}Ni_{8.6}Be_{26.25}$ and $Zr_{46.75}Ti_{8.25}Cu_{7.5}Ni_{10}Be_{27.5}$ BMGs respectively.

Presently calculated elastic properties for $Zr_{44}Ti_{11}Cu_{10}Ni_{10}Be_{25}$ and $Zr_{38.5}Ti_{16.5}Cu_{15.25}Ni_{9.75}Be_{25}$ BMG are listed in **Tables 4** and **5** respectively. From this table, one can see that the results are obtained due to T, IU and F screening functions are very close to one another as compared to the H screening function. Due to lack of experimental data and other information of elastic

Properties	H [13]	T [14]	IU [15]	F [16]	S [17]	Exp. [5, 6]	Other [4–6]
$\upsilon_L \times 10^5$ (cm s^{-2})	4.634	5.266	5.265	5.294	4.866	—	5.182
$\upsilon_T \times 10^5$ (cm s^{-2})	2.675	3.040	3.0403	3.056	2.810	—	2.487
$B_T \times 10^{12}$ (dyne/cm^2)	0.641	0.828	0.828	0.836	0.707	1.134	1.137 1.119
$G \times 10^{12}$ (dyne/cm^2)	0.385	0.497	0.496	0.502	0.424	0.352	0.476 0.372
ξ	0.25	0.25	0.25	0.25	0.25	0.35	0.352
$Y \times 10^{12}$ (dyne/cm^2)	0.961	1.242	1.241	1.255	1.060	0.957	1.039 1.005
θ_D (K)	334.7	380.4	380.4	380.4	351.5	—	327

Table 4. Elastic properties for $Zr_{46.75}Ti_{14}Cu_{12.5}Ni_{10}Be_{22.5}$ BMG.

Properties	H [13]	T [14]	IU [15]	F [16]	S [17]	Exp.	Other
$\upsilon_L \times 10^5$ (cm s^{-2})	4.544	5.171	5.180	5.207	4.765	—	—
$\upsilon_T \times 10^5$ (cm s^{-2})	2.624	2.986	2.991	3.006	2.751	—	—
$B_T \times 10^{12}$ (dyne/cm^2)	0.643	0.832	0.835	0.843	0.706	—	—
$G \times 10^{12}$ (dyne/cm^2)	0.386	0.499	0.509	0.506	0.424	—	—
ξ	0.25	0.25	0.25	0.25	0.25	—	—
$Y \times 10^{12}$ (dyne/cm^2)	0.964	1.248	1.252	1.265	1.059	—	—
θ_D (K)	332.5	378.3	379.1	380.9	348.7	—	—

Table 5. Elastic properties of $Zr_{44}Ti_{11}Cu_{10}Ni_{10}Be_{25}$ BMG.

properties. So we do not offer any concrete remark at this stage, but it is sure that this data is very useful for the further investigation.

3.2. $Zr_{52.25}$-$Cu_{28.5}$-$Ni_{4.75}$-$Al_{9.5}$-Ta_5 BMG

Here, Our well established model potential is used along with five different types of local field correction functions due to H, T, IU, F and S for to generate the pair potential for $Zr_{52.25}Cu_{28.5}Ni_{4.75}Al_{9.5}Ta_5$ BMG [4] system. **Figure 5** shows the calculated pair potential for $Zr_{52.25}Cu_{28.5}Ni_{4.75}Al_{9.5}Ta_5$ BMG [4]. It is observed that the depth of the pair potential obtained using model potential is highly affected. This depth affects the height and peak of the pair correlation functions. This pair potential is helping to compute phonon frequencies of longitudinal and transverse branch and it is shown in **Figure 6(b)**. No experimental data and other available data are found for comparison for sound velocities. So, we do not put any concert comment on sound velocity at this point.

The absence of experimental data and other information on elastic properties like bulk modulus, Poisson ratio and Debye temperature, so that, present results are compared with calculated values and other available results [5]. From the **Table 7**, it is observed that F function is in good agreement with the calculated values and other available results [5]. On the other hand,

Properties	H [13]	T [14]	IU [15]	F [16]	S [17]	Exp.	Other
$\upsilon_L \times 10^5$ (cm s^{-2})	4.347	4.942	4.954	4.954	4.561	—	—
$\upsilon_T \times 10^5$ (cm s^{-2})	2.510	2.853	2.860	2.880	2.633	—	—
$B_T \times 10^{12}$ (dyne/cm^2)	0.614	0.793	0.797	0.805	0.675	—	—
$G \times 10^{12}$ (dyne/cm^2)	0.368	0.476	0.478	0.483	0.405	—	—
ξ	0.25	0.25	0.25	0.25	0.25	—	—
$Y \times 10^{12}$ (dyne/cm^2)	0.920	1.189	1.196	1.208	1.013	—	—
θ_D (K)	322.0	366.1	367.0	368.9	337.9	—	—

Table 6. Elastic properties of $Zr_{38.5}Ti_{16.5}Cu_{15.25}Ni_{9.75}Be_{25}$ BMG.

Properties	H [13]	T [14]	IU [15]	F [16]	S [17]	Exp.	Other [5]
$\upsilon_L \times 10^5$ (cm s^{-2})	3.5505	4.0124	4.0041	4.4025	3.7471	—	—
$\upsilon_T \times 10^5$ (cm s^{-2})	2.0499	2.3166	2.3118	2.324	2.1634	—	—
$B_T \times 10^{12}$ (dyne/cm^2)	0.4879	0.6230	0.6205	0.6271	0.5434	—	—
$G \times 10^{12}$ (dyne/cm^2)	0.2927	0.3738	0.3723	0.3762	0.3260	—	—
ξ	0.25	0.25	0.25	0.25	0.25	—	—
$Y \times 10^{12}$ (dyne/cm^2)	0.7317	0.9346	0.9307	0.9406	0.8151	—	0.90
θ_D (K)	253.57	286.56	285.97	287.48	267.61	—	—

Table 7. Elastic properties of $Zr_{52.25}Cu_{28.5}Ni_{4.75}Al_{9.5}Ta_5$ BMG.

Young modulus and Shear modulus using T, IU and S local field correction functions are in good agreement with the results mention in Ref. [5].

3.3. Zr_{57}-Ti_5-Cu_{20}-Ni_8-Al_{10} BMG

Here, it has been reported for the first time to generate the pair potential for the $Zr_{57}Ti_5Cu_{20}Ni_8Al_{10}$ BMG system. The computed pair potential is shown in **Figure 7(a)** using present model potentials. In this case, the computed pair potential is affected by type of screening used. The pair potential computed using model potential shows first positive minimum. The depth of this minimum is affected by type of screening used and almost at the r value where pair potential shows a positive minimum. The computed pair potential is greatly affected by model potential.

Using a pair potential it has been projected the longitudinal and transverse phonon frequencies for $Zr_{57}Ti_5Cu_{20}Ni_8Al_{10}$ BMG are shown in **Figure 7(b)**. From the **Figure 7(b)** it is understood from the results of phonon frequencies that the nature of peak positions are not much exaggerated by different screening functions, but both the longitudinal and transverse frequencies show small deviation for H, T and S functions with respect to IU and F screening function in **Figure 7(b)**.

On the other hand, the transverse modes undergo larger thermal modulation due to the anharmonicity of the vibrations in the BMGs. In the long wavelength limit, the dispersion curves are linear and confirming characteristics of elastic waves. The PDC for transverse phonons attain maxima at a higher q value than the longitudinal phonon curve. At present calculated elastic properties for $Zr_{57}Ti_5Cu_{20}Ni_8Al_{10}$ BMG are listed in **Table 8**. From **Table 8**, one can see that by using the T, IU and F screening functions, the results are very close to one another as compared to the H screening function. Modulus of rigidity 'G', Young modulus 'Y' and Debye temperature is showing the better agreement with experimental values [5, 6] computed using the T, IU and F screening while obtains due to H and S show the underestimate values than the experimental and other available data. We are sure that this data is very useful for the further investigation.

Properties	H [13]	T [14]	IU [15]	F [16]	S [17]	Exp. [4–6]	Other [4–6]
$\upsilon_L \times 10^5$ (cm s^{-2})	3.2622	3.6125	3.6212	3.6375	3.3707	4.623	—
$\upsilon_T \times 10^5$ (cm s^{-2})	1.8834	2.0857	2.0907	2.1001	1.9461	2.149	—
$B_T \times 10^{12}$ (dyne/cm^2)	0.3867	0.4738	0.47608	0.4804	0.4125	0.992	—
$G \times 10^{12}$ (dyne/cm^2)	0.2318	0.2843	0.2857	0.2882	0.2475	0.301	0.301
ξ	0.25	0.25	0.25	0.25	0.25	—	—
$Y \times 10^{12}$ (dyne/cm^2)	0.5795	0.7107	0.7141	0.7206	0.6188	0.82	0.82
θ_D (K)	233.70	258.79	259.92	260.58	241.47	270.3	270.1

Table 8. Elastic properties of $Zr_{57}Ti_5Cu_{20}Ni_8Al_{10}$ BMG.

http://dx.doi.org/10.5772/intechopen.79568

3.4. Zr-Al-Ni-Cu BMG ($Zr_{61.88}Al_{10}Ni_{10.12}Cu_{18}$, $Zr_{64.13}Al_{10}Ni_{10.12}Cu_{15.15}$, $Zr_{65}Al_{10}Ni_{10}Cu_{15}$)

Our well recognized model potential is used along with five different local field correction function for the generate pair potential for $Zr_{61.88}Al_{10}Ni_{10.12}Cu_{18}$, $Zr_{64.13}Al_{10}Ni_{10.12}Cu_{15.75}$ and $Zr_{65}Al_{10}Ni_{10}Cu_{15}$ BMG system. From **Figures 8(a)**, **9(a)** and **10(a)** it is observed that the study reveals the general trends of the pair potential in all cases, suggesting that the position of the first minimum depth in the pair potential in the present study is obtained due to F screening function.

Using this pair potential it has been computed the longitudinal and transverse phonon frequency for $Zr_{61.88}Al_{10}Ni_{10.12}Cu_{18}$, $Zr_{64.13}Al_{10}Ni_{10.12}Cu_{15.75}$ and $Zr_{65}Al_{10}Ni_{10}Cu_{15}$ BMG are shown in **Figures 8(b)**, **9(b)** and **10(b)** respectively. Phonon mode graphs show that the nature of peak position is not much affected by different type of screening functions. The longitudinal and transverse frequencies show deviation for H, T and S functions with respect to F screening for Zr-Al-Ni-Cu BMG systems. It is obvious from the figures that the oscillations are protruding in the longitudinal mode as compared to transverse mode, which indicates that collective excitations at larger wave vector transfer due to the dispersion of longitudinal excitation. The influence of the results of phonon frequencies is clearly observed on the elastic constants, as we have calculated these elastic constants from the long wavelength limit of phonon frequencies.

From the **Tables 9–11** it is observed that sound velocity computed using present model potential along with T, IU and F functions are found to be very close to one another and calculated sound velocities using F screening function shows a good agreement with available data [4–6]. Computed bulk modulus using model potential along with all local field correction functions is underestimated as compared to the experimental [4] and other available data [5, 6]. Presently computed percentile deviation for modulus of rigidity with respect to available data. The maximum deviation is found in F screening function, the values are 25.5, 26.9 and 6.2% for $Zr_{61.88}Al_{10}Ni_{10.12}Cu_{18}$, $Zr_{64.13}Al_{10}Ni_{10.12}Cu_{15.75}$ and $Zr_{65}Al_{10}Ni_{10}Cu_{15}$ respectively, and minimum deviation is found for in H function, the values are found 2.57 and 4.0% for $Zr_{61.88}Al_{10}Ni_{10.12}Cu_{18}$ and $Zr_{64.13}Al_{10}Ni_{10.12}Cu_{15.75}$ respectively.

Presently calculated Young's modulus and Debye temperature using local model potential along with the S screening function is found in good agreement with available results for

Properties	H [13]	T [14]	IU [15]	F [16]	S [17]	Exp. [6]	Other [6]
$\upsilon_L \times 10^5$ (cm s^{-2})	3.6701	4.1883	4.1731	4.1990	3.8565	4.693	4.704
$\upsilon_T \times 10^5$ (cm s^{-2})	2.1189	2.4181	2.4043	2.4243	2.2265	2.046	2.092
$B_T \times 10^{12}$ (dyne/cm^2)	0.4975	0.6479	0.6432	0.6513	0.5493	1.077	1.083
$G \times 10^{12}$ (dyne/cm^2)	0.2985	0.3888	0.3899	0.3908	0.3296	0.293	0.291
ξ	0.25	0.25	0.25	0.25	0.25	0.375	0.37
$Y \times 10^{12}$ (dyne/cm^2)	0.7463	0.9719	0.9649	0.9769	0.8240	0.805	0.801
θ_D (K)	263.355	300.544	299.451	301.31	276.73	0.263	262.9

Table 9. Elastic properties of $Zr_{61.88}Al_{10}Ni_{10.12}Cu_{18}$ BMG.

Properties	H [13]	T [14]	IU [15]	F [16]	S [17]	Exp.	Other [6]
$\upsilon_L \times 10^5$ (cm s^{-2})	3.6694	3.4202	4.1873	4.2100	3.8666	—	4.679
$\upsilon_T \times 10^5$ (cm s^{-2})	2.1186	2.4262	2.4175	2.4306	2.2324	—	2.079
$B_T \times 10^{12}$ (dyne/cm^2)	0.4940	0.6479	0.6432	0.6502	0.5481	—	1.066
$G \times 10^{12}$ (dyne/cm^2)	0.2964	0.3887	0.3859	0.3901	0.5481	—	0.285
ξ	0.25	0.25	0.25	0.25	0.25	—	0.37
$Y \times 10^{12}$ (dyne/cm^2)	0.7410	0.9718	0.9649	0.9754	0.8227	—	0.785
θ_D (K)	261.2	299.1	298.06	299.68	275.24	—	259.2

Table 10. Elastic properties of $Zr_{64.13}Al_{10}Ni_{10.12}Cu_{15.75}$ BMG.

Properties	H [13]	T [14]	IU [15]	F [16]	S [17]	Exp. [4–6]	Other [4–6]
$\upsilon_L \times 10^5$ (cm s^{-2})	3.3964	3.9328	3.9199	3.9440	3.6025	—	5.050
$\upsilon_T \times 10^5$ (cm s^{-2})	1.9609	2.2706	2.2632	2.2771	2.0799	—	2.393
$B_T \times 10^{12}$ (dyne/cm^2)	0.4086	0.5478	0.5443	0.5510	0.4597	1.067	1.066 1.034 1.120
$G \times 10^{12}$ (dyne/cm^2)	0.2452	0.3267	0.3265	0.3306	0.2758	0.31	0.303 0.359
ξ	0.25	0.25	0.25	0.25	0.25	—	0.35
$Y \times 10^{12}$ (dyne/cm^2)	0.6129	0.8218	0.8164	0.8265	0.6895	0.791	0.83
θ_D (K)	238.2	275.9	274.9	276.6	252.7	267	267 292.9

Table 11. Elastic properties of $Zr_{65}Al_{10}Ni_{10}Cu_{15}$ BMG.

$Zr_{61.88}Al_{10}Ni_{10.12}Cu_{18}$, and $Zr_{64.13}Al_{10}Ni_{10.12}Cu_{15.75}$ and IU function is found in good agreement with experimental as well as other available results [6]. On the other hand, the calculated values of Young's modulus and Debye temperature using model potential along with T, IU and F screening functions are found very close to each other and good agreement with the other theoretical data for Zr-Al-Ni-Cu BMG system.

4. Conclusion

The dispersion of longitudinal phonon shows oscillatory behavior for the large q values while lack of thereof in the transverse phonons. The transverse phonon frequencies increase with wave number and get saturated at the first peak of $\omega_T \rightarrow q$ curves with small variations. The $\omega \rightarrow q$ curve for the transverse phonons achieves maxima at a higher q value than the longitudinal phonon curve. The peak heights of the longitudinal as well as transverse phonon frequencies of these BMGs are nearly the same. Thus, the dispersion curves of these BMGs are found to be similar.

It is apparent from the $\omega_L \rightarrow q$ curves of the glassy materials that they are screening sensitive in the low-momentum region. The difference in $\omega \rightarrow q$ relation begins right from the starting value of q and it's becomes maximum at the first peak of the $\omega_L \rightarrow q$ curve, again, it tends to decrease and both $\omega_L \rightarrow q$ relations seem to converge at the first minima of the $\omega_L \rightarrow q$ curve. The position of the first peak is independent of the screening functions. However, the height of the peak strongly depends on the type of screening employed in the present calculations. The phonon dispersion curve for the Zr-based bulk metallic glasses computed using the IU and F function give higher numerical values than other local field correction functions. Using H-function give the lowest values for the Zr-base bulk metallic glasses. Agarwal has done the longitudinal and transverse modes for the Zr-Ti-Cu-Ni-Be for three different concentrations using the BS-Method. When compared with our present approach, it is found that model potential gives underestimated results.

Presently calculated elastic properties for BMGs are listed in **Tables 2–11**. It is observed that the computed elastic properties using model potential are in excellent agreement with experimental and other available theoretical data. Among the five different screening functions T, IU and F functions show good agreement for present model potential. While due to H screening function than the other LFCF and computed values using S lying between the F and H screening function. For Zr-Ti-Cu-Ni-Be, Zr-Cu-Ni-Al-Ta, Zr-Ti-Cu-Ni-Al and Zr-Al-Ni-Al BMGs at different concentrations computed using model potential, it is observed that ν_l and ν_t, Young modulus, modulus rigidity, Debye temperature using the T, IU, F and S local field correction functions show the very good agreement with experimental and other available data. The Zr-based BMGs are observed that the present results obtained due to T, IU and F screening functions are in good agreement with available with other data. Present study clearly reveals that proper description of local field correction function is required for the study of phonon modes of bulk metallic glasses.

Overall, we stated that the phonon dispersion curve generated from the HB approach reproduces satisfactorily the general characteristic of dispersion curves. The well recognized Model potential along with IU, Farid et al. [F] and Sarkar-Sen et al. [S] local field correction functions generates consistent results. Hence, our Model-1 potential is suitable for the studying the phonon dynamics of bulk metallic glasses.

Author details

Punitkumar Harshadbhai Suthar

Address all correspondence to: sutharpunit@rediffmail.com

Department of Physics, CU Shah Science College, Ahmedabad, Gujarat, India

References

[1] Klement W, Willens RH, Duwez P. Non crystalline structure in solidified Gold-Silicon Alloy. Nature. 1960;**187**:869

[2] Johnson WL. Crystal to glass tranformation in metallic material. Progress in Materials Science. 1986;**30**:81

[3] Grrer AL. Metallic glasses. Current Opinion in Solid State & Materials Science. 1997;**2**:412

[4] Wang WH, Dong C, Shek CH. Bulk metallic glasses. Materials Science & Engineering R: Reports. 2004;**44**:45

[5] Wang WH. Correlation between elastic moduli and properties in bulk metallic glasses. Journal of Applied Physics. 2006;**99**:093506

[6] Wang WH. The elastic properties, elastic models and elastic perspectives of metallic glasses. Progress in Materials Science. 2012;**57**:487

[7] Hui X, Fang HZ, Chen GL, Shang SL, Wang Y, Liu ZK. Icosahedral ordring in $Zr_{41}Ti_{14}Cu_{12.5}Ni_{10}Be_{22.5}$ bulk metallic glass. Applied Physics Letters. 2008;**92**:201913

[8] Agarwal PC. Phonon dispersion in Zr-Ti-Cu-Ni-Be bulk metallic glasses. Physics B. 2006; **381**:239

[9] Perker A, Johnson WL. A highly processable metallic glass: $Zr_{41}Ti_{14}Cu_{12.5}Ni_{10}Be_{22.5}$. Applied Physics Letters. 1993;**63**:2342

[10] Jonson WL. Bulk Glass-Forming Metallic Alloys: Science and Technology. MRS Bulletin. 1999;**24**:42

[11] Bhatia AB, Singh RN. Phonon dispersion in metallic glass - A simple model. Physical Review B. 1985;**31**:4751

[12] Habbard J, Beeby JL. Collective motion in liquids. Journal of Physics C. 1971;**45**:331

[13] Harrison WA. Pseudopotential in the Theory of Metal. New York: W A Benamin Inc; 1966

[14] Taylor R. A simple, useful analytical form of static electron gas dielectric function. Journal of Physics F. 1981;**8**:1699

[15] Ichimaru S, Utsumi K. Analytic expression for the dielectric screening function of strongly coupled electron liquid at metallic and lower densities. Physics Review. 1978;**24**:3220

[16] Farid B, Heine V, Engel GE, Robertson IJ. Extremal properties of the Harris-Foulkes functional and improved screening caluation for the electron gas. Physical Review B. 1993; **48**:11602

[17] Sarkar A, Sen DS, Roy HD. Static local field factor for Dielectric screening function of electron gas at metallic and lower densities. Modern Physics Letters. 1998;**12**:639

[18] Takeno S, Goda M. A Theory of phonon-like excitations in non-crystalline solids and liquids. Progress in Theoretical Physics. 1971;**47**:790

[19] Jani AR, Gajjar PN, Patel HK. Suceptibility of some simple metals by local pesudopotentials. Physica Status Solidi B. 1991;**105**:169

[20] Thakor PB, Gajjar PN, Jani AR. Structure of some at Rare-Earth liquid metals - A charged hard sphere approach. Communications in Mathematical Physics. 2004;**14**:15

[21] Thakore BY, Gajjar PN, Jani AR. Collective modes in $Ca_{70}Mg_{30}$ Glass. Bulletin of Materials Science. 2000;**23**:5

[22] Suthar PH. Study of certain physical properties of some alkaline earth metals, some transition metals and their alloys and bulk metallic glasses using pseudopotential theory. [PhD thesis]. Sardar Patel University; 2012

[23] Thakore BY, Khambholja SG, Suthar PH, Bhatt NK, Jani AR. Collective modes and elastic constants of liquid $Al_{83}Cu_{17}$ binary alloy. Chinese Physics Letters. 2010;**27**(9):096203

[24] Suthar PH, Gajjar PN, Thakore BY, Jani AR. Study of phonon modes and elastic properties of $Sc_{36}Al_{24}Co_{20}Y_{20}$ and $Gd_{36}Al_{24}Co_{20}Y_{20}$ bulk metallic glasses. Journal of Physics: Conference Series. 2013;**423**(1):012030

[25] Suthar PH. Phonon dispersion relation of Mg-Cu-Gd bulk metallic glasses. AIP Conference Proceedings. 2016;**1728**:020599

IntechOpen